Supporting information

Maximizing the Peroxidase-Like Activity of Pd@Pt_xRu_{4-x} Nanocubes by Precisely Controlling the Shell Thickness and Their Application in Colorimetric Biosensors

Yiming Jiang,[a] Jiawei Zhu,[b] Li Li,[a] Yahui Gao,[a] Juncai Leng,[a] Jiai Yan,[c] Shuoming Liu,[a] Feng Zhang,[c] Han Liu,[a] Chenlu Zhu,[a] Lichun Guo,[a] Haijiao Xie,[d] Wei Zhao[a*]

[a] *State Key Laboratory of Food Science and Technology, School of Food Science and Technology, Jiangnan University, Wuxi, Jiangsu 214122, P. R. China*

[b] *School of Chemical and Material Engineering, Jiangnan University, Wuxi, Jiangsu 214122, P. R. China*

[c] *Affiliated Hospital of Jiangnan University, Wuxi, Jiangsu 214122, P. R. China*

[d] *Hangzhou Yanqu Information Technology Co., Ltd., Xixi Legu Creative Pioneering Park, No. 712 Wen'er West Road, Xihu District, Hangzhou, Zhejiang 310003, P. R. China*

[*]**Corresponding author:** Prof. Wei Zhao, Email: zhaow@jiangnan.edu.cn

Supporting Figures

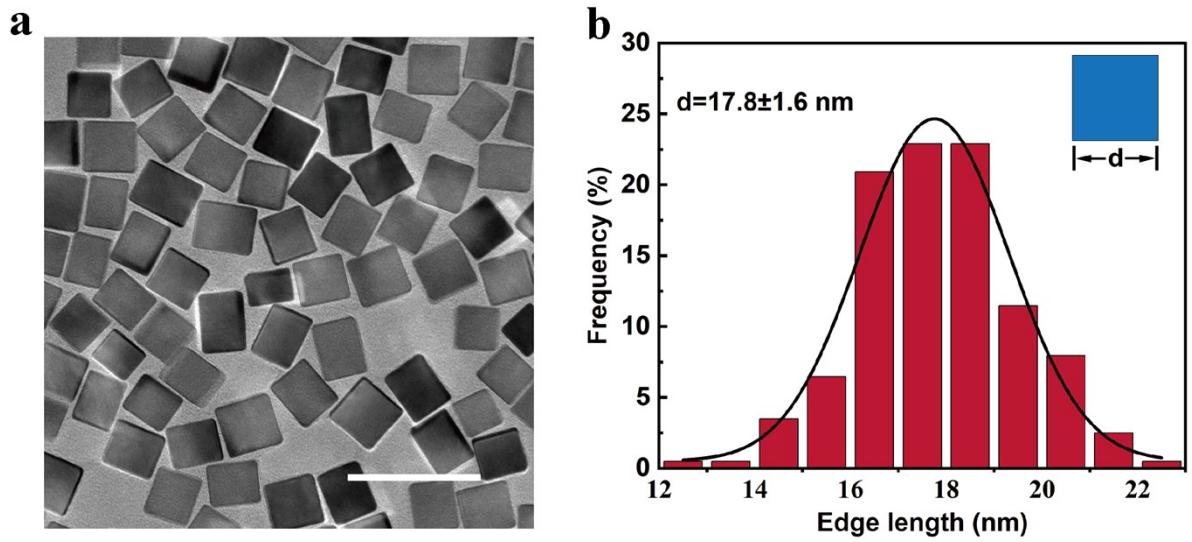

Figure S1. (**a**) TEM image (scale bar: 50 nm) and (**b**) size distribution of the Pd cubic core. The average edge lengths of 17.8±1.6 nm was derived from about two hundred particles.

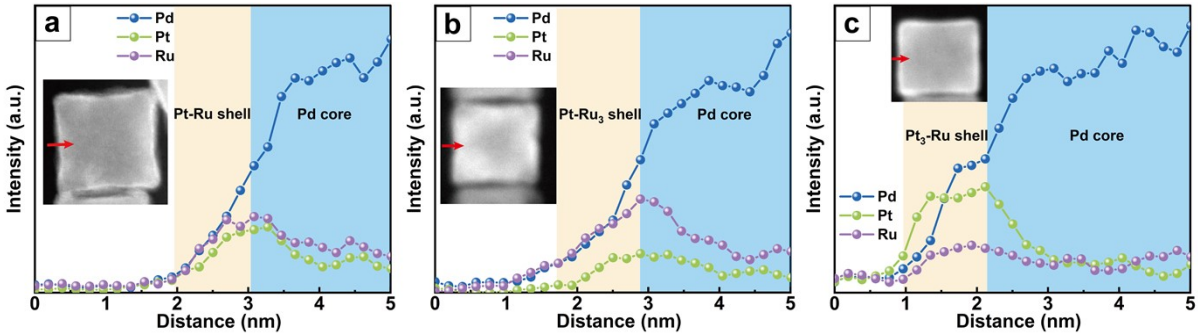

Figure S2. (**a-c**) EDX line scan analysis of an individual (**a**) Pd@Pt-$Ru_{3.3L}$, (**b**) Pd@Pt-Ru_3, (**c**) Pd@Pt_3-Ru nanocrystal along the red arrow.

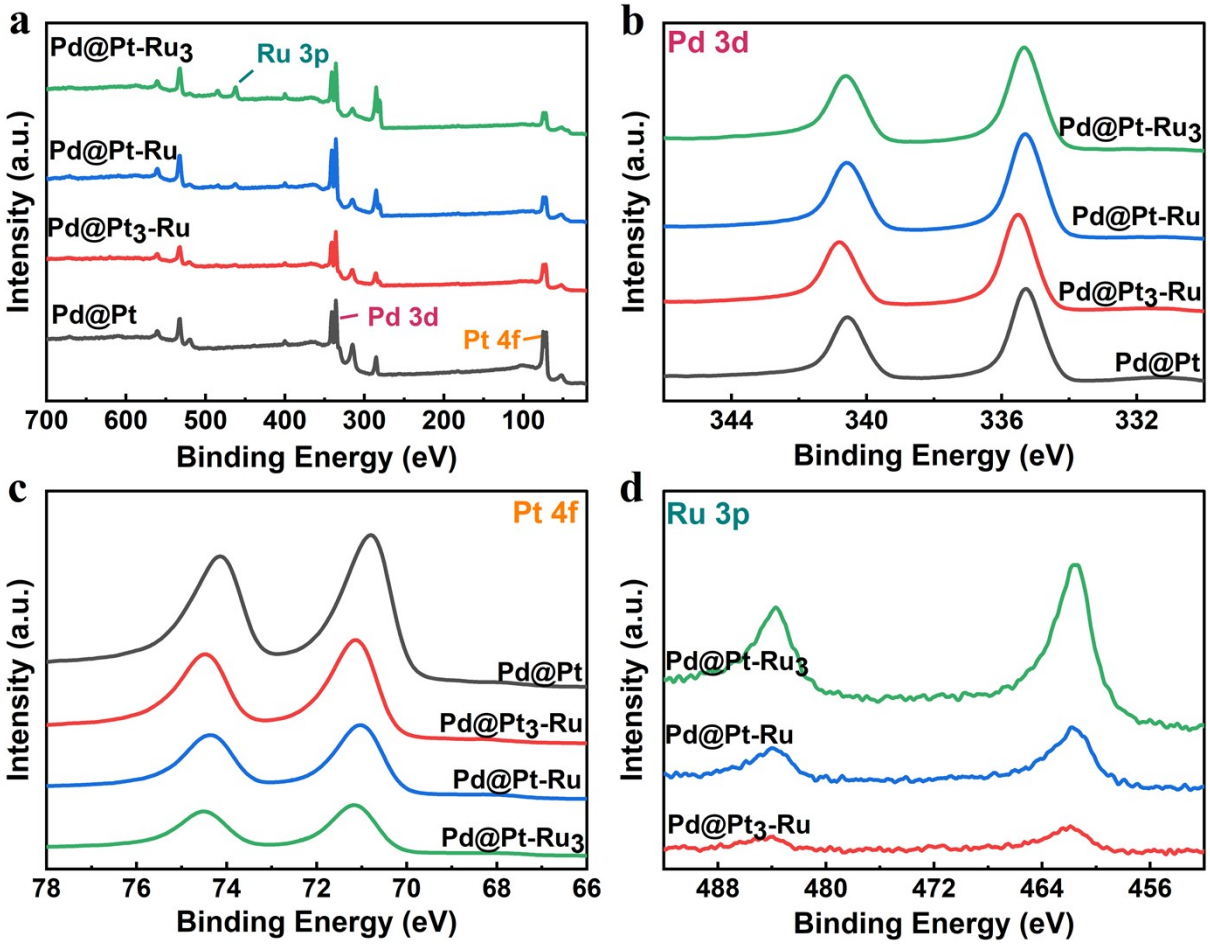

Figure S3. XPS spectra for the (**a**) survey scan, (**b**) Pd 3d, (**c**) Pt 4f, and (**d**) Ru 3p of different nanocrystals.

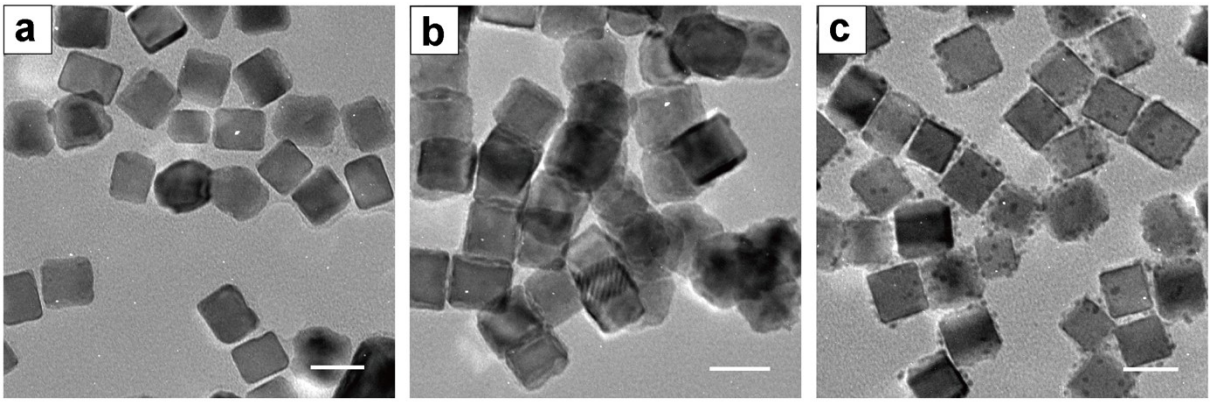

Figure S4. TEM images of Pd@Pt-$Ru_{3.3L}$ core-shell nanocrystals synthesized by using the standard protocol, except for (**a**) using lower reaction temperature (120 ^{o}C), (**b**) using a faster-injecting rate (50 mL·h^{-1}), and (**c**) the absence of KBr in the reaction solution. All scale bars are 20 nm.

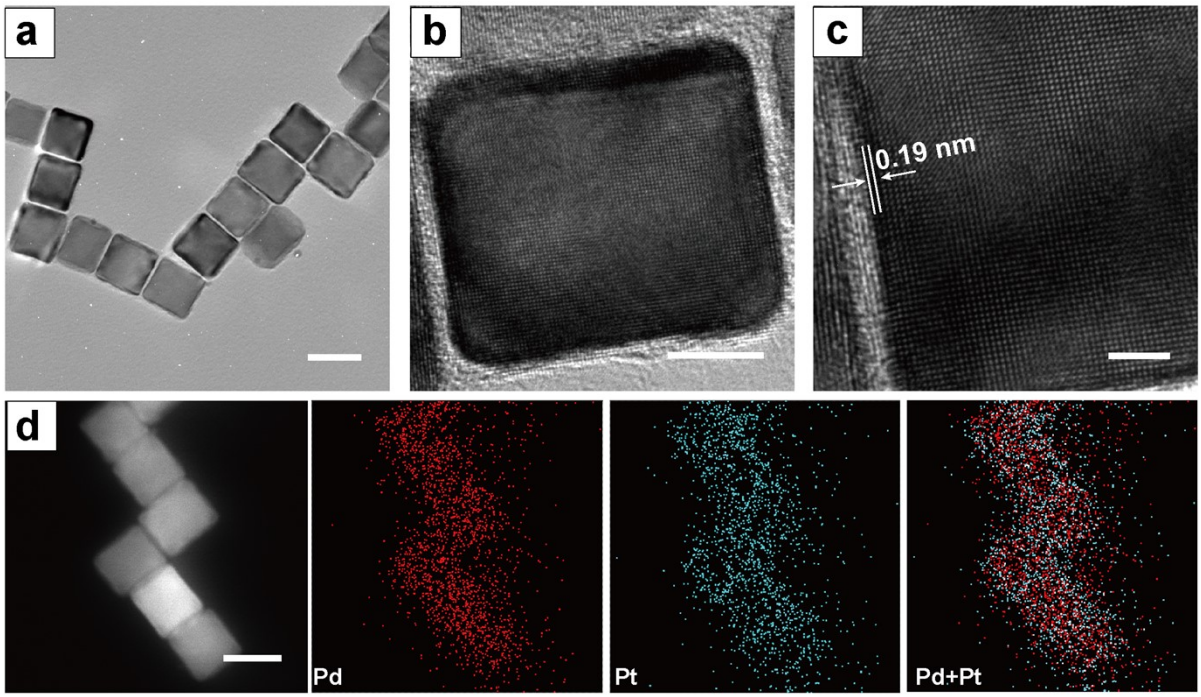

Figure S5. (**a**) TEM image of Pd@Pt nanocrystals (scale bar: 20 nm), (**b**) High-resolution TEM (HRTEM) image of an individual Pd@Pt nanocrystal (scale bar: 5 nm), (**c**) HRTEM image taken from the shell of nanocrystal in (**b**) (scale bar: 2 nm), and (**d**) STEM image and EDX elemental mapping of Pd@Pt nanocubes (scale bar: 20 nm), confirming the Pd@Pt core-shell nanocrystals.

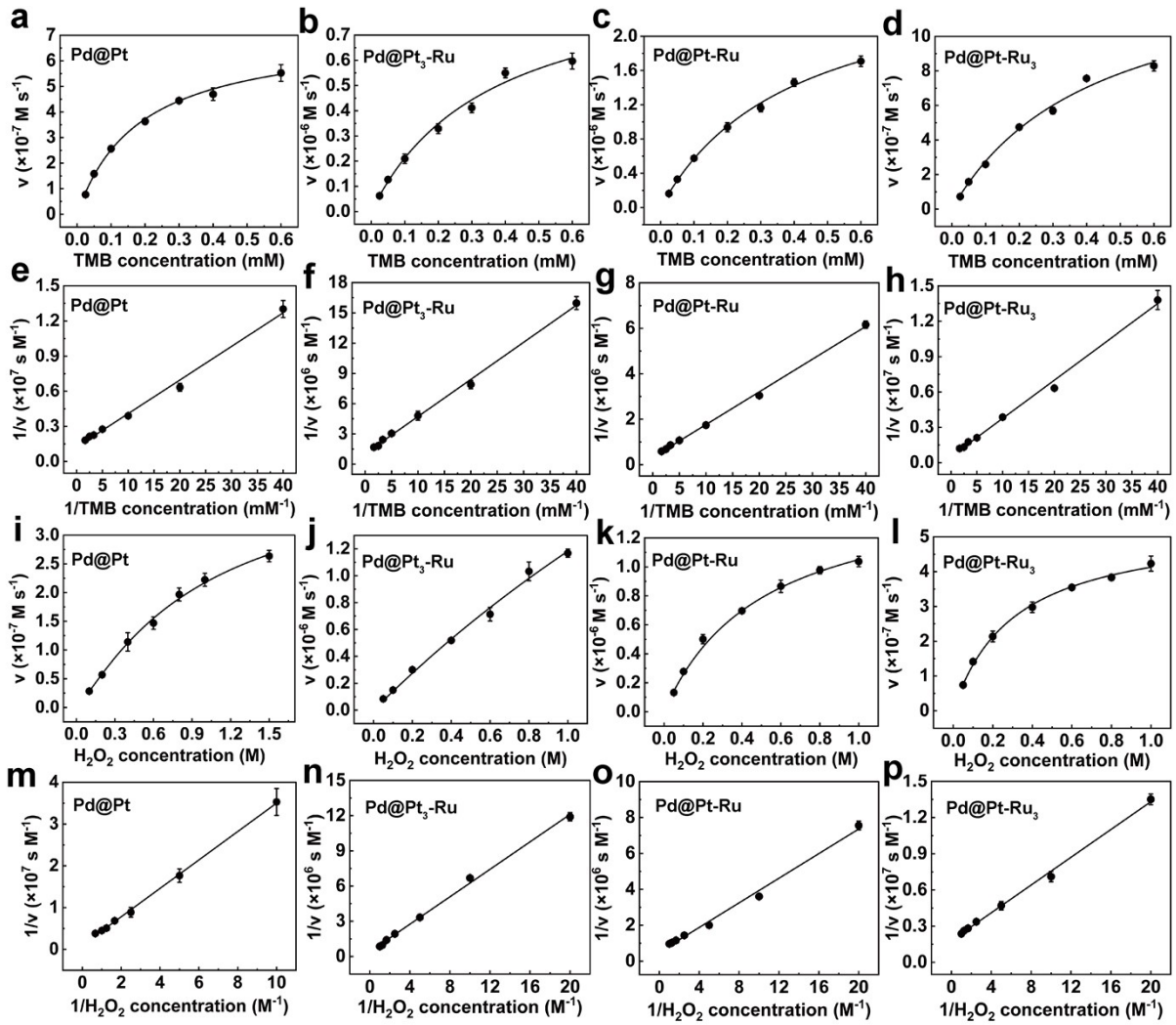

Figure S6. Steady-state kinetic assays of catalysts with different Pt/Ru molar ratios for the oxidation of TMB in the presence of H_2O_2. (**a-h**) and (**i-p**) indicated kinetic assays towards TMB and H_2O_2 as a substrate, in which H_2O_2 and TMB concentrations were fixed at 2.0 M and 0.8 mM, respectively. Typical Michaelis−Menten curves for: (**a, i**) Pd@Pt NPs; (**b, j**) Pd@Pt_3-Ru NPs; (**c, k**) Pd@Pt-Ru NPs; (**d, l**) Pd@Pt-Ru_3 NPs. The Double-reciprocal plots for (**e-h**) and (**m-p**) were generated from (**a-d**) and (**i-l**), respectively. Error bar represents the standard deviations of three independent assays.

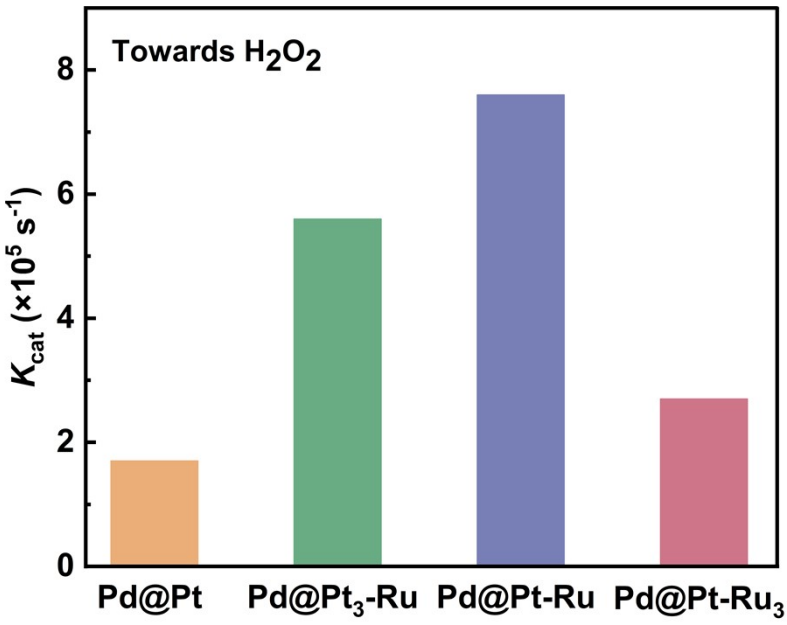

Figure S7. The K_{cat} toward H_2O_2 for core-shell nanocrystals with different Pt/Ru ratios.

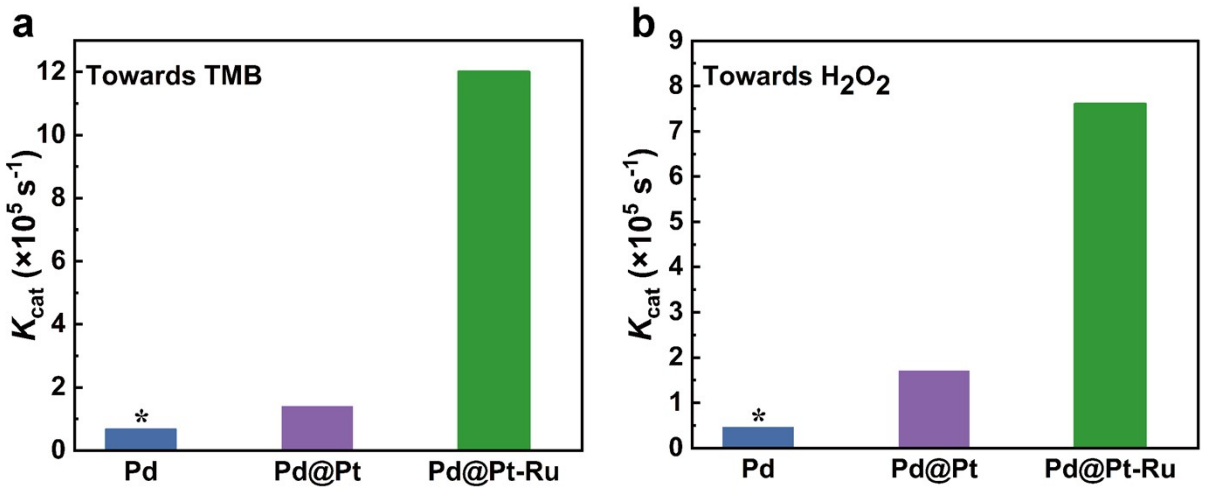

Figure S8. The histograms comparing K_{cat} toward (**a**) TMB and (**b**) H_2O_2 of Pd@Pt-$Ru_{3.3L}$ cubes relative to initial Pd cubes and Pd@Pt cubes. *Data obtained from Ref S2.

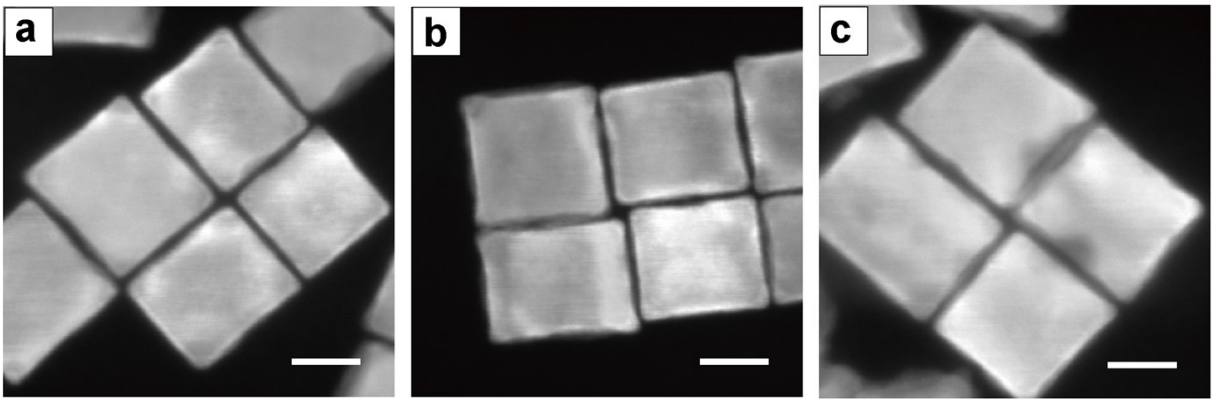

Figure S9. HAADF-STEM images of the Pd@Pt-Ru_{nL} core-shell nanocubes with different numbers of Pt-Ru bimetallic overlayers, where n = 1.4, 2.2, and 4.6 for samples in (**a-c**), respectively (scale bars: 10 nm).

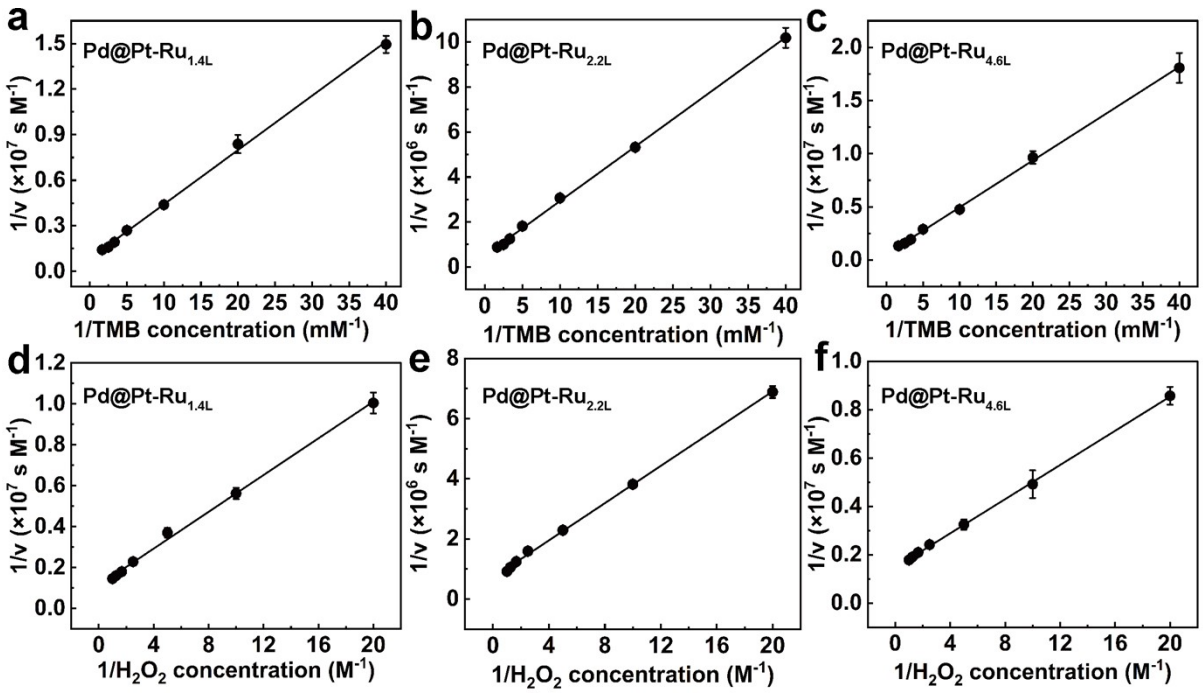

Figure S10. Steady-state kinetic assays of Pd@Pt-Ru_{nL} (n: the number of Pt-Ru alloy atomic overlayer). Error bar indicated the standard deviation of three independent measurements. (**a-c**) and (**d-f**) showed the double-reciprocal plots towards TMB and H_2O_2, respectively, for (**a, d**) Pd@Pt-$Ru_{1.4L}$; (**b, e**) Pd@Pt-$Ru_{2.2L}$; (**c, f**) Pd@Pt-$Ru_{4.6L}$.

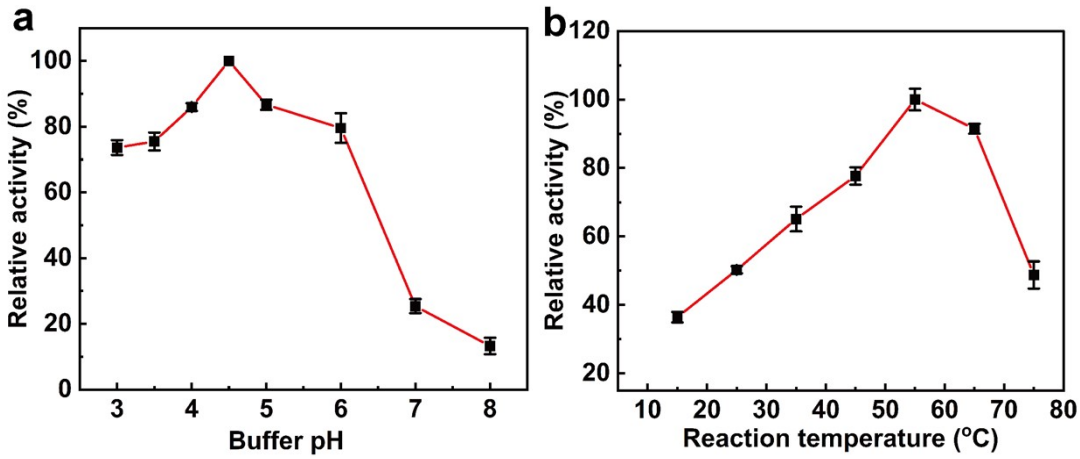

Figure S11. The effects of environmental conditions such as (**a**) buffer pH and (**b**) reaction temperature on the catalytic activity of Pd@Pt-$Ru_{3.3L}$ catalysts.

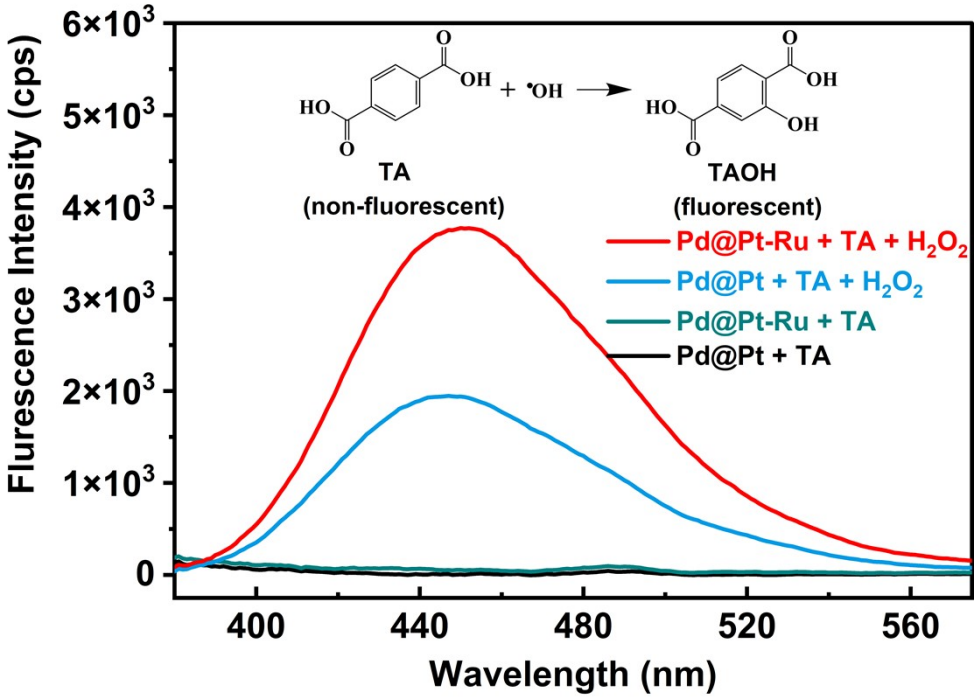

Figure S12. The detection of hydroxyl radical (•OH) generated from Pd@Pt-$Ru_{3.3L}$ and Pd@Pt catalysts using TA as a probe.

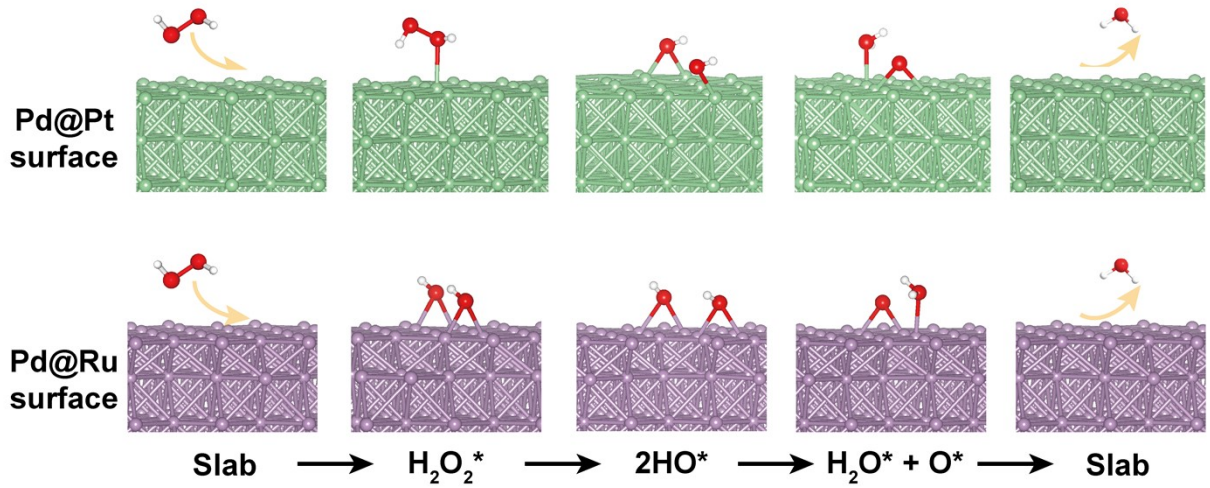

Figure S13. The optimized H_2O_2 adsorption and dissociation configurations on Pt and Ru surfaces, respectively.

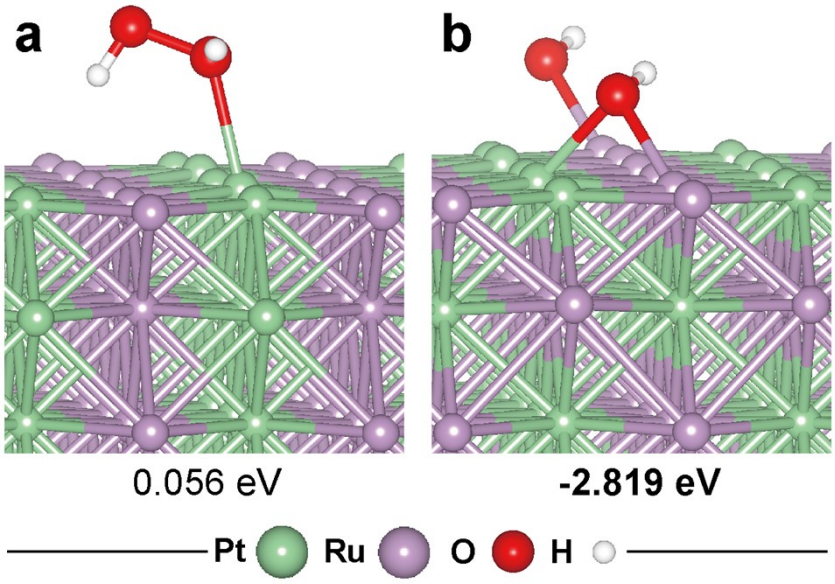

Figure S14. The adsorption configurations of H_2O_2 over (a) Pt site and (b) Ru site of Pd@Pt-Ru system. Values below each model represent the corresponding adsorption energy for the H_2O_2 molecule, where the most stable model is shown in bold. Additionally, a similar adsorption configuration of H_2O_2 on the Ru atom is observed in Ref S21.

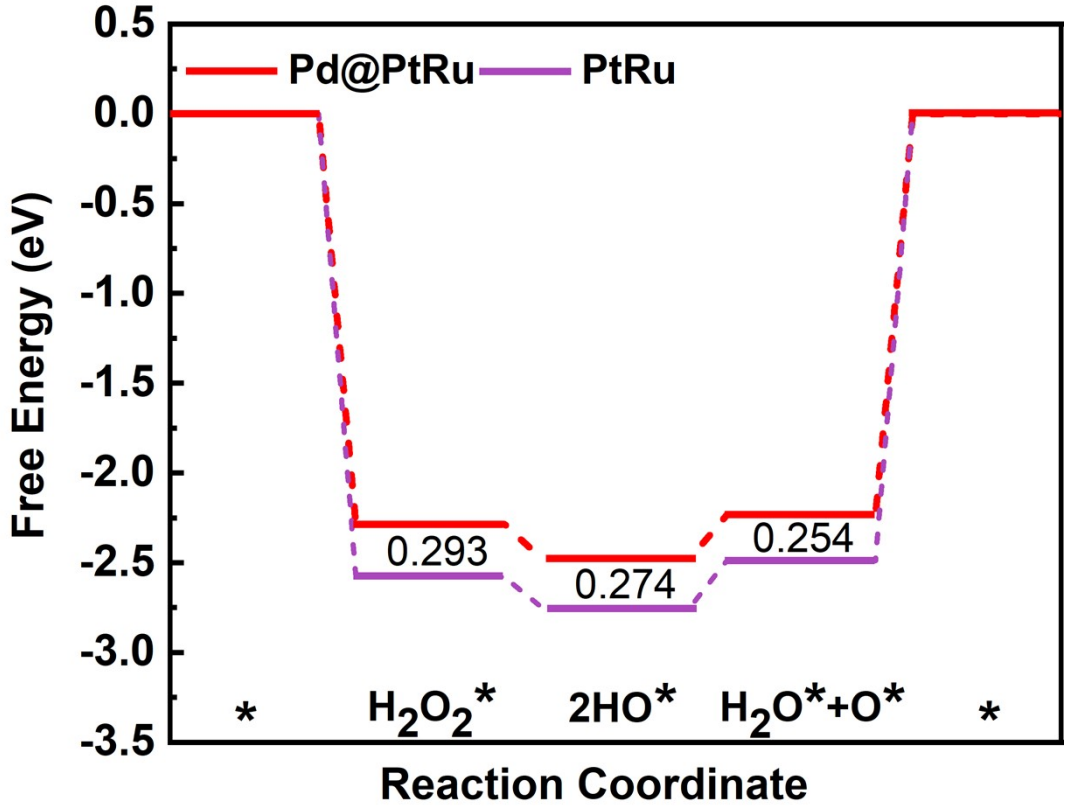

Figure S15. Energy profiles for H_2O_2 decomposition over the surface of Pd@Pt-Ru and Pt-Ru structures. The values represent the difference between two structures for each reaction step.

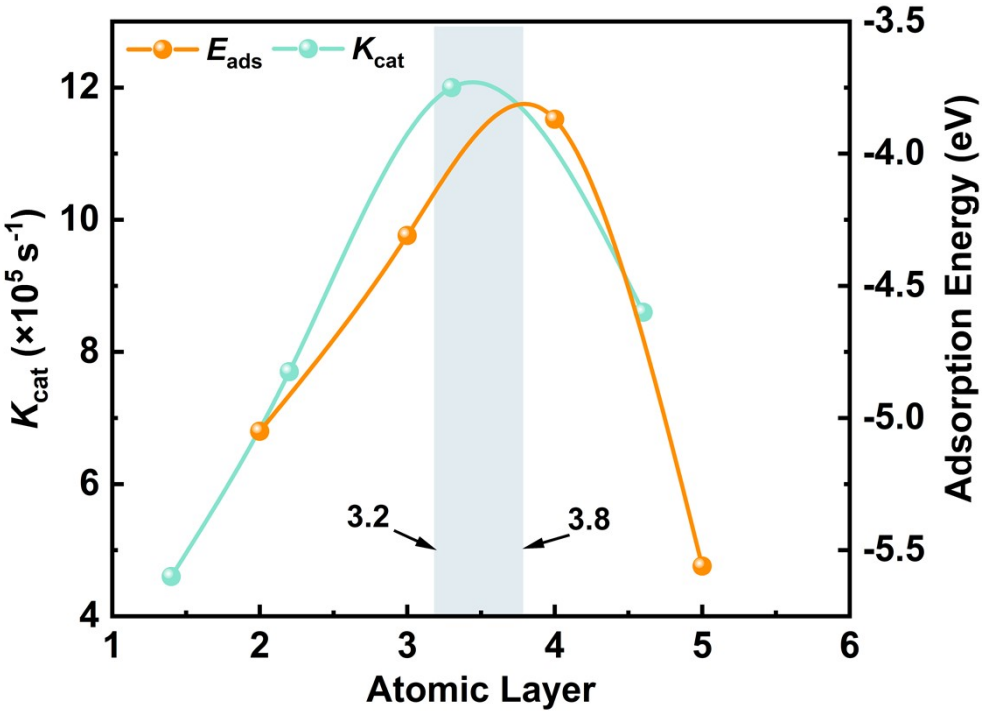

Figure S16. Analysis of the E_{ads} (2OH) of Pt-Ru$_{nL}$/Pd(100) slab models using DFT calculations.

Supporting Tables

Table S1. The molar ratio of PGMs (%) and the average number of atomic layers in shells for different nanocrystals determined by ICP-MS data.

Samples	Molar ratio of Pd/Pt/Ru (%)	Mass ratio of Pd/Pt/Ru (%)	Average number of atomic layers in shells
Pd@Pt	81.1/18.9	70.1/29.9	3.4
Pd@Pt_3-Ru	79.8:15.1:5.1	71.0/24.6/4.4	3.6
Pd@Pt-Ru	82.5:9.4:8.1	76.6/16.1/7.3	3.3
Pd@Pt-Ru_3	79.5:5.8:14.7	76.1/10.3/13.6	3.5

Table S2. Comparison of the kinetic parameters of different nanocrystals towards TMB and H_2O_2. [*E*] represents the particle concentration of catalysts, K_m is the Michaelis constant, V_{max} is maximal reaction velocity, K_{cat} represents the catalytic constant that equals V_{max}/[E].

Catalyst	[*E*] (M)	Substance	K_m (M)	V_{max} (M s^{-1})	K_{cat} (s^{-1})	Refs
Pd@Pt	6.1×10^{-12}	TMB	2.4×10^{-4}	8.2×10^{-7}	1.4×10^{5}	This
	6.1×10^{-12}	H_2O_2	3.4×10^{0}	1.0×10^{-6}	1.7×10^{5}	work
Pd@Pt_3-Ru	2.2×10^{-12}	TMB	3.5×10^{-4}	9.6×10^{-7}	4.4×10^{5}	This
	4.4×10^{-12}	H_2O_2	1.4×10^{0}	2.5×10^{-6}	5.6×10^{5}	work
Pd@Pt-Ru	2.6×10^{-12}	TMB	4.5×10^{-4}	3.1×10^{-6}	1.2×10^{6}	This
	2.6×10^{-12}	H_2O_2	5.8×10^{-1}	2.0×10^{-6}	7.6×10^{5}	work
Pd@Pt-Ru_3	2.1×10^{-12}	TMB	6.3×10^{-4}	2.0×10^{-6}	9.5×10^{5}	This
	2.1×10^{-12}	H_2O_2	3.2×10^{-1}	5.5×10^{-7}	2.7×10^{5}	work
HRP	2.5×10^{-11}	TMB	4.3×10^{-4}	1.0×10^{-7}	4.0×10^{3}	S1
	2.5×10^{-11}	H_2O_2	3.7×10^{-3}	8.7×10^{-8}	3.5×10^{3}	

Table S3. Comparison of the kinetic parameters of Pd@Pt-Ru_{nL} (n: the number of Pt-Ru alloy atomic overlayers) nanocubes towards TMB and H_2O_2. [*E*] represents the particle concentration of catalysts, K_m is the Michaelis constant, V_{max} is maximal reaction velocity, K_{cat} represents the catalytic constant that equals V_{max}/[*E*].

Catalyst	**[*E*] (M)**	**Substance**	K_m **(M)**	V_{max} **(M s^{-1})**	K_{cat} **(s^{-1})**
Pd@Pt-$Ru_{1.4L}$	2.6×10^{-12}	TMB	4.2×10^{-4}	1.2×10^{-6}	4.6×10^{5}
		H_2O_2	4.0×10^{-1}	8.9×10^{-7}	3.4×10^{5}
Pd@Pt-$Ru_{2.2L}$	2.6×10^{-12}	TMB	4.9×10^{-4}	2.0×10^{-6}	7.7×10^{5}
		H_2O_2	4.3×10^{-1}	1.4×10^{-6}	5.4×10^{5}
Pd@Pt-$Ru_{3.3L}$	2.6×10^{-12}	TMB	4.5×10^{-4}	3.1×10^{-6}	1.2×10^{6}
		H_2O_2	5.8×10^{-1}	2.0×10^{-6}	7.6×10^{5}
Pd@Pt-$Ru_{4.6L}$	2.1×10^{-12}	TMB	8.0×10^{-4}	1.8×10^{-6}	8.6×10^{5}
		H_2O_2	2.4×10^{-1}	6.8×10^{-7}	3.2×10^{5}

Table S4. Comparison of the kinetic parameters of different catalysts towards TMB and H_2O_2. [*E*] represents the particle concentration of catalysts, K_m is the Michaelis constant, V_{max} is maximal reaction velocity, K_{cat} represents the catalytic constant that equals $V_{max}/[E]$.

Catalyst	Size (nm)	[*E*] (M)	Substance	K_m (M)	V_{max} (M s^{-1})	K_{cat} (s^{-1})	Refs
HRP	-	2.5×10^{-11}	TMB	4.3×10^{-4}	1.0×10^{-7}	4.0×10^{3}	S1
		2.5×10^{-11}	H_2O_2	3.7×10^{-3}	8.7×10^{-8}	3.5×10^{3}	
Fe_3O_4 particles	300 (diameter)	1.1×10^{-12}	TMB	9.8×10^{-5}	3.4×10^{-8}	3.0×10^{4}	S1
		1.1×10^{-12}	H_2O_2	1.5×10^{-1}	9.8×10^{-8}	8.6×10^{4}	
Pd cubes	18 (edge length)	1.4×10^{-12}	TMB	5.4×10^{-5}	9.7×10^{-8}	6.9×10^{4}	S2
		1.4×10^{-12}	H_2O_2	7.0×10^{-1}	6.5×10^{-8}	4.6×10^{4}	
Pd-Ir cubes	19.2 (edge length)	3.4×10^{-14}	TMB	1.3×10^{-4}	6.5×10^{-8}	1.9×10^{6}	S2
		3.4×10^{-14}	H_2O_2	3.4×10^{-1}	5.1×10^{-8}	1.5×10^{6}	
Graphene oxide sheets	1 (thickness)	1.2×10^{-9} [a]	TMB	2.4×10^{-5}	3.5×10^{-8}	2.9×10^{1}	S3
		1.2×10^{-9} [a]	H_2O_2	4.0×10^{-3}	3.9×10^{-8}	3.3×10^{1}	
Co_3O_4 cubes	20 (edge length)	3.4×10^{-10}	TMB	3.7×10^{-5}	6.3×10^{-8}	1.8×10^{2}	S4
		3.4×10^{-10}	H_2O_2	1.4×10^{-1}	1.2×10^{-7}	3.5×10^{2}	
$Pt_{48}Pd_{52}$-Fe_3O_4 particles	~12 (diameter)	3.9×10^{-9} [b]	TMB	7.9×10^{-5}	9.4×10^{-8}	2.4×10^{1}	S5
		3.9×10^{-9} [b]	H_2O_2	-	-	-	
Prussian blue-Fe_2O_3 particles	~10 (diameter)	3.1×10^{-10}	TMB	3.1×10^{-4}	1.1×10^{-6}	3.4×10^{3}	S6
		3.1×10^{-10}	H_2O_2	3.2×10^{-1}	1.2×10^{-6}	3.8×10^{3}	
Pd@Pt	~40	1.9×10^{-12}	TMB	8.7×10^{-5}	6.2×10^{-8}	3.1×10^{4}	S7

nanoplates	(edge length)	1.9×10^{-12}	H_2O_2	2.2×10^{-3}	5.0×10^{-8}	2.5×10^{4}	
$Au@Pt_{0.25}$	20×70	1.7×10^{-11}	TMB	2.6×10^{-5}	9.6×10^{-8}	5.7×10^{3}	S8
rods	(w×l)	1.7×10^{-11}	H_2O_2	-	-	-	
Pd@Pt	~9	1.3×10^{-12}	TMB	4.8×10^{-4}	7.1×10^{-7}	5.5×10^{5}	S9
cubes	(edge length)	1.3×10^{-12}	H_2O_2	3.9×10^{-1}	4.2×10^{-7}	3.2×10^{5}	
Au@Pd	~20	9.6×10^{-11}	TMB	1.7×10^{-4}	2.0×10^{-6}	2.1×10^{4}	S10
particles	(diameter)	9.6×10^{-11}	H_2O_2	1.1×10^{0}	4.4×10^{-6}	4.6×10^{4}	
Irregular-	~5-7 nm	8.1×10^{-11}	TMB	1.2×10^{-4}	1.3×10^{-6}	2.3×10^{4}	S11
Pt particles	(diameter)	8.1×10^{-11}	H_2O_2	7.7×10^{-1}	1.9×10^{-6}	1.6×10^{4}	
Ru	6.2	1.1×10^{-11}	TMB	6.0×10^{-5}	1.3×10^{-7}	1.3×10^{4}	S12
nanocages	(edge length)	1.1×10^{-11}	H_2O_2	3.2×10^{-1}	7.4×10^{-8}	7.0×10^{3}	
PVP/PtRu	3.5	2.1×10^{-9} [c]	TMB	7.6×10^{-4}	7.5×10^{-6}	3.6×10^{3}	S13
particles	(diameter)	2.1×10^{-9} [c]	H_2O_2	3.6×10^{-2}	3.7×10^{-6}	1.8×10^{3}	
PVP_{55}-Pt	6.5	5.9×10^{-13}	TMB	6.6×10^{-4}	3.9×10^{-7}	6.5×10^{5}	S14
cubes	(edge length)	5.9×10^{-13}	H_2O_2	-	-	-	
Pt	14.6	8.2×10^{-13}	TMB	4.8×10^{-4}	7.9×10^{-7}	9.7×10^{5}	S15
particle	(diameter)	8.2×10^{-13}	H_2O_2	-	-	-	
High-index	44	2.5×10^{-14}	TMB	-	1.5×10^{-7}	6.0×10^{6}	S16
facet Pt cubes	(edge length)	2.5×10^{-14}	H_2O_2	-	1.3×10^{-7}	5.1×10^{6}	
Pt	48	3.5×10^{-14}	TMB	-	5.6×10^{-8}	1.6×10^{6}	S16
nanospheres	(diameter)	3.5×10^{-14}	H_2O_2	-	4.7×10^{-8}	1.4×10^{6}	
Pt	3	3.4×10^{-7} [d]	TMB	9.6×10^{-5}	1.4×10^{-7}	4.1×10^{-1}	S17

nanoclusters	(diameter)	3.4×10^{-7} [d]	H_2O_2	3.1×10^{-3}	1.8×10^{-7}	5.3×10^{-1}	
AuPt	2.5	9.5×10^{-9} [e]	TMB	-	-	-	S18
nanodots	(diameter)	9.5×10^{-9} [e]	H_2O_2	1.1×10^{-3}	4.3×10^{-8}	4.5×10^{0}	
Pt hollow	20	7.0×10^{-6}	TMB	8.1×10^{-4}	1.2×10^{-7}	1.7×10^{-2}	S19
nanodendrites	(length)	7.0×10^{-6}	H_2O_2	6.9×10^{-3}	9.9×10^{-8}	1.4×10^{-2}	
Porous Pt/Ag	~21	1.2×10^{-11} [f]	TMB	2.5×10^{-4}	1.1×10^{-7}	9.2×10^{3}	S20
nanoparticles	(edge length)	1.2×10^{-11} [f]	H_2O_2	3.5×10^{-4}	1.6×10^{-7}	1.4×10^{4}	
Pd@Pt	~20	6.1×10^{-12}	TMB	2.4×10^{-4}	8.2×10^{-7}	1.4×10^{5}	This
nanocrystals	(edge length)	4.4×10^{-12}	H_2O_2	3.4×10^{0}	1.0×10^{-6}	1.7×10^{5}	work
Pd@Pt-$Ru_{3.3L}$	~20	2.6×10^{-12}	TMB	4.5×10^{-4}	3.1×10^{-6}	1.2×10^{6}	This
nanocrystals	(edge length)	2.6×10^{-12}	H_2O_2	5.8×10^{-1}	2.0×10^{-6}	7.6×10^{5}	work

[a] Estimated from the mass concentration (40 μg/mL) and the hypothesis that each catalyst is an ideal layered structure with a particle size of 100×1 nm (diameter × thickness).

[b] Converted from the particle concentration (3.5×10^{12} particles in 1.5 mL of reaction solution).

[c] Estimated from the final concentration (0.44 μg/mL) and the hypothesis that each catalyst is an ideal spherical structure with a size of 3.53 nm (diameter).

[d] Estimated from the final concentration (0.5 mg/mL) and the hypothesis that each catalyst is an ideal spherical structure with a size of 3.0 nm (diameter).

[e] Estimated from the final concentration (8 μg/mL) and the hypothesis that each catalyst is an ideal spherical structure with a size of 2.5 nm (diameter).

[f] Estimated from the final concentration (3.9 μg/mL) and the hypothesis that each catalyst is an ideal octahedral structure with a size of 21 nm (edge length).

References:

S1. L. Gao, J. Zhuang, L. Nie, J. Zhang, Y. Zhang, N. Gu, T. Wang, J. Feng, D. Yang, S. Perrett, X. Yan, *Nat. Nanotechnol*. **2007**, 2, 577.

S2. X. Xia, J. Zhang, N. Lu, M.J. Kim, K. Ghale, Y. Xu, E. McKenzie, J. Liu, H. Ye, *ACS Nano*. **2015**, 9, 9994.

S3. Y. Song, K. Qu, C. Zhao, J. Ren, X. Qu, *Adv. Mater*. **2010**, 22, 2206.

S4. J. Mu, Y. Wang, M. Zhao, L. Zhang, *Chem. Commun.* **2012**, 48, 2540.

S5. X. Sun, S. Guo, C. Chung, W. Zhu, S. Sun, *Adv. Mater*. **2013**, 25, 132.

S6. X. Zhang, S. Gong, Y. Zhang, T. Yang, C. Wang, N. Gu, *J. Mater. Chem.* **2010**, 20, 5110.

S7. J. Wei, X. Chen, S. Shi, S. Mo, N. Zheng, *Nanoscale* **2015**, 7, 19018.

S8. J. Liu, X. Hua, S. Hou, T. Wen, W. Liu, X. Zhu, J. Yin, X. Wu, *Sens. Actuators B, Chem*. **2012**, 166, 708.

S9. E. Davidson, X. Zhang, Z. Gao, X. Xia, *Sens. Int*. **2020**, 1, 100031.

S10. Z. Gao, L. Hou, M. Xu, D. Tang, *Sci. Rep*. **2014**, 4, 3966.

S11. Z. Gao, M. Xu, L. Hou, G. Chen, D. Tang, *Anal. Chim. Acta.* **2013**, 776, 79.

S12. H. Ye, J. Mohar, Q. Wang, M. Catalano, M.J. Kim, X. Xia, *Sci. Bull*. **2016**, 61, 1739.

S13. Y. Park, P. Gupat, V. Tran, S. Son, W. Hur, H. Lee, J. Park, S. Kim, G. Seong, *Colloids Surf. B.* **2021**, 204, 111783.

S14. H. Ye, Y. Liu, A. Chhabra, E. Lilla, X. Xia, *ChemNanoMat*. **2017**, 3, 33.

S15. Z. Xi, K. Wei, Q. Wang, M. Kim, S. Sun, V. Fung, X. Xia, *J. Am. Chem. Soc*. **2021**, 143, 2660.

S16. Z. Gao, S. Lv, M. Xu, D. Tang, *Analyst*. **2017**, 142, 911.

S17. L. Jin, Z. Meng, Y. Zhang, S. Cai, Z. Zhang, C. Li, L. Shang, Y. Shen, *ACS Appl. Mater. Interfaces*. **2017**, 9, 10027.

S18. S. Zhang, Q. Lu, F. Wang, Z. Xiao, L. He, D. He, L. Deng, *ACS Appl. Mater. Interfaces*. **2021**, 13, 37535.

S19. R. Wu, Y. Chong, G. Fang, X. Jiang, Y. Pan, C. Chen, J. Yin, C. Ge, *Adv. Funct. Mater.* **2018**, 28, 1801484.

S20. S. Cai, X. Jia, Q. Han, X. Yan, R. Yang, C. Wang, *Nano Res*. **2017**, 10, 2056.

S21. J. Zhang, T. Wu, H. Thang, K. Tseng, X. Hao, B. Xu, H. Chen, Y. Peng, *Small*, **2022**, 18, 2104844.